ECE 797:

Speech and Audio Processing

Hand-out for Lecture #3

Thursday, January 29, 2004

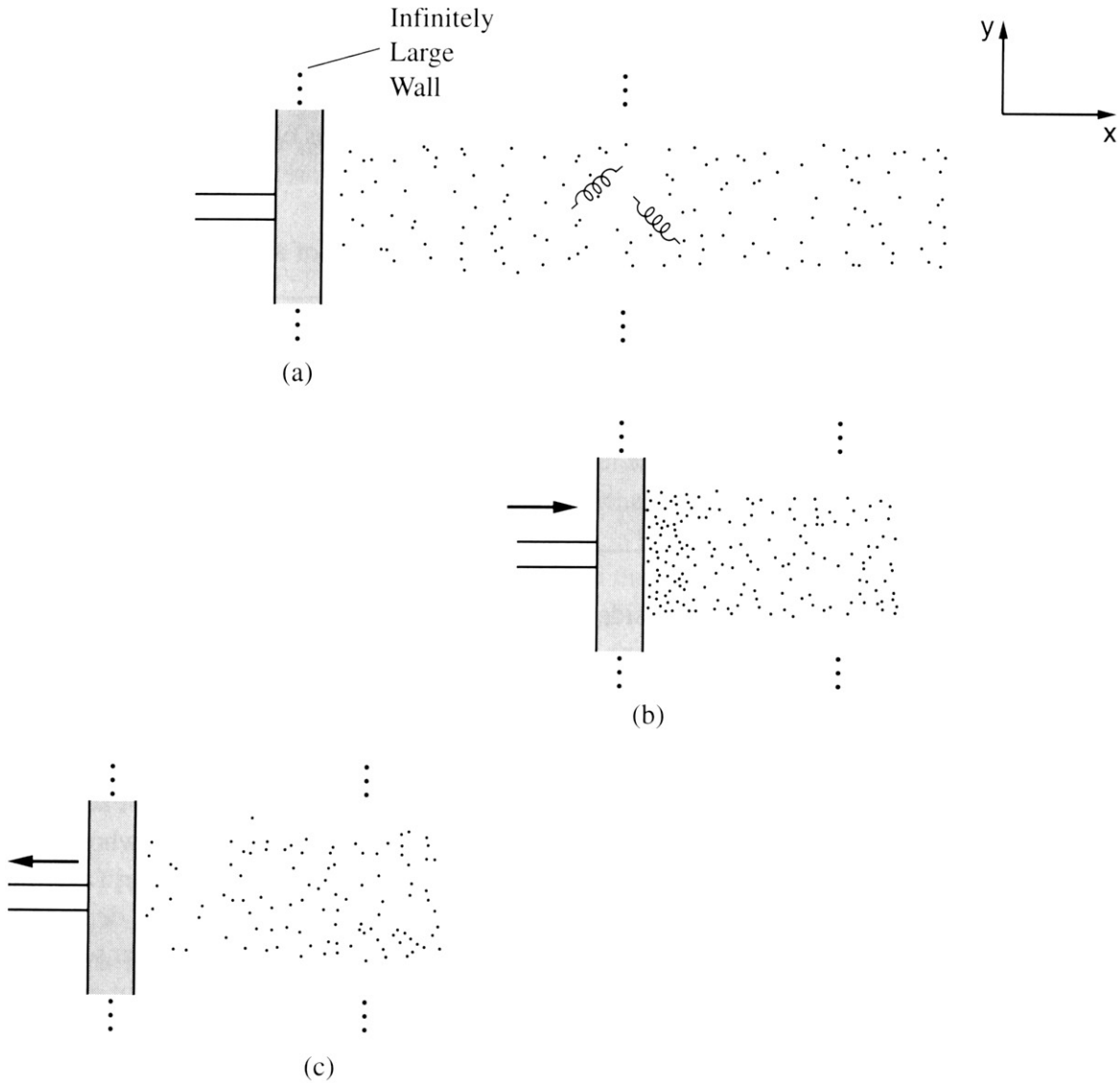

Figure 4.1 Compression and rarefaction of air particles in front of an infinitely large wall: (a) illustration of springiness among air particles; (b) compression; (c) rarefaction.

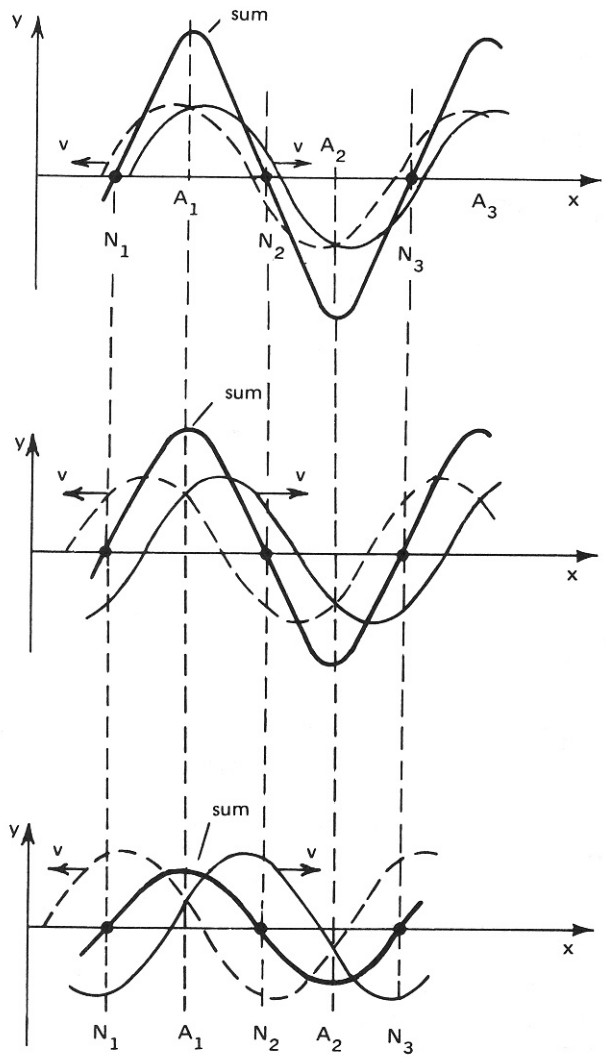

FIGURE 3.11 Superposition of two transverse waves of the same amplitude and frequency, moving in mutually *opposite* directions +V and −V. The resulting wave pattern does not propagate: it remains "anchored" at the nodes *N*, changing only its amplitude.

(Roederer, 1994)

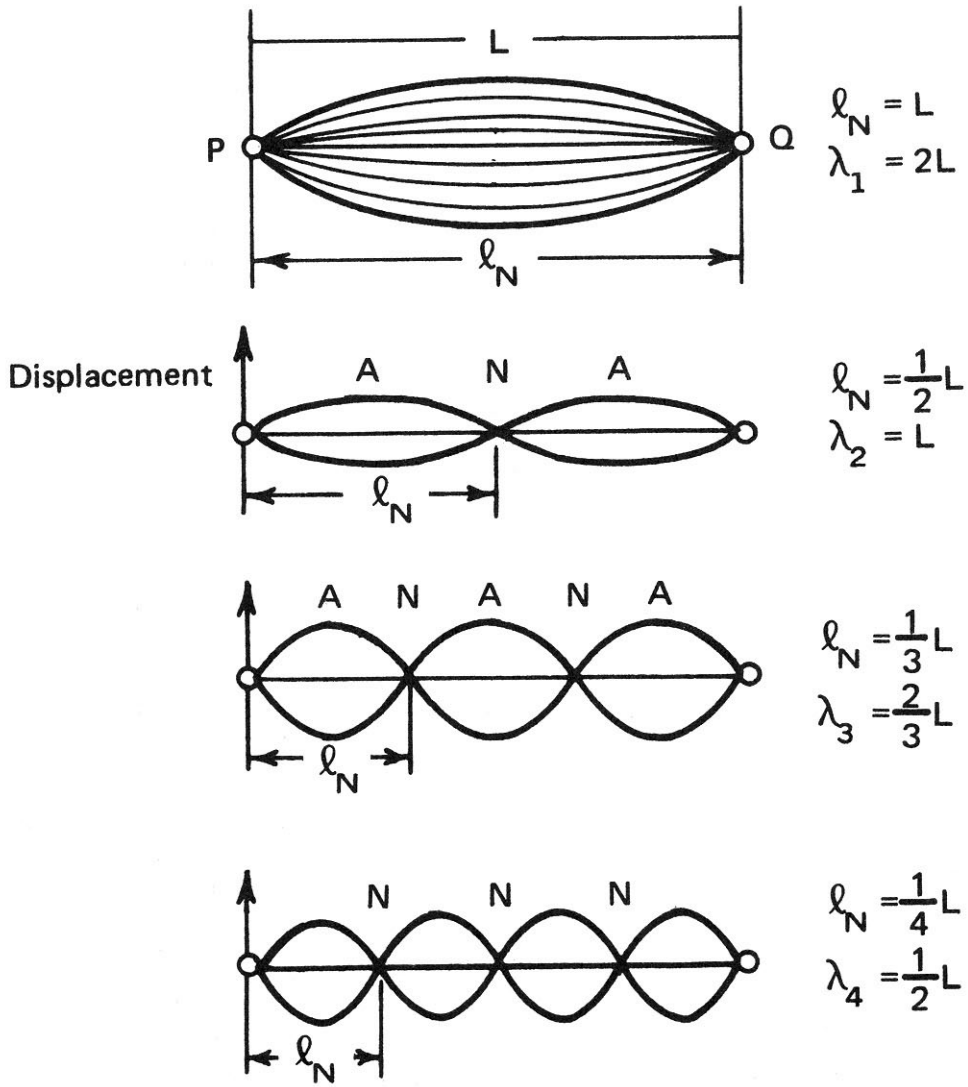

FIGURE 4.2 Standing wave modes in a vibrating string.

(Roederer, 1994)

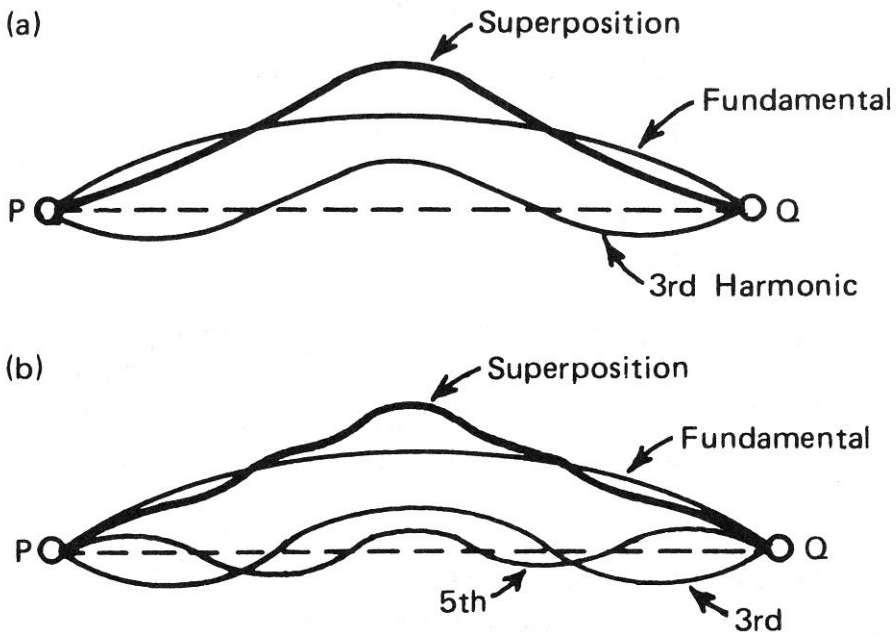

FIGURE 4.7 Superposition of two (a) and three (b) harmonics selected so as to approximate the triangular shape shown in Fig. 4.6.

(Roederer, 1994)

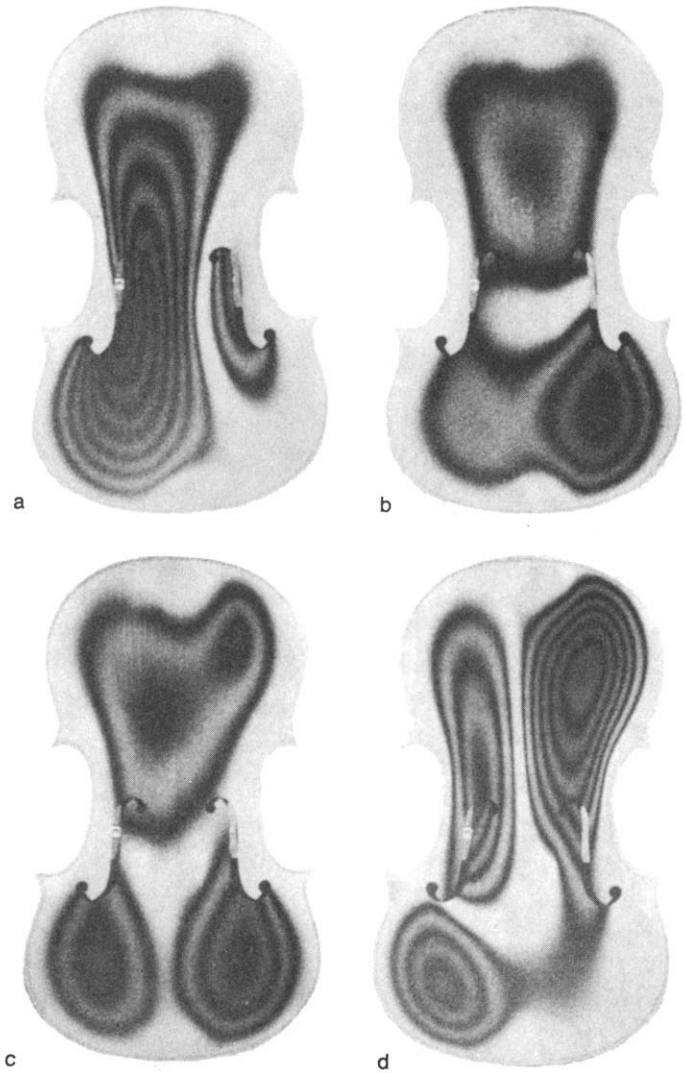

FIGURE 4.13 Holograms depicting the first four vibration modes of the top plate of a violin (with *f* holes and mounted sound post, without fingerboard). Each one of the dark curves represents a contour of equal deformation amplitude. (a) 540 Hz; (b) 775 Hz; (c) 800 Hz; (d) 980 Hz. Reprinted by permission from Jansson et al., 1970.

(Roederer, 1994)

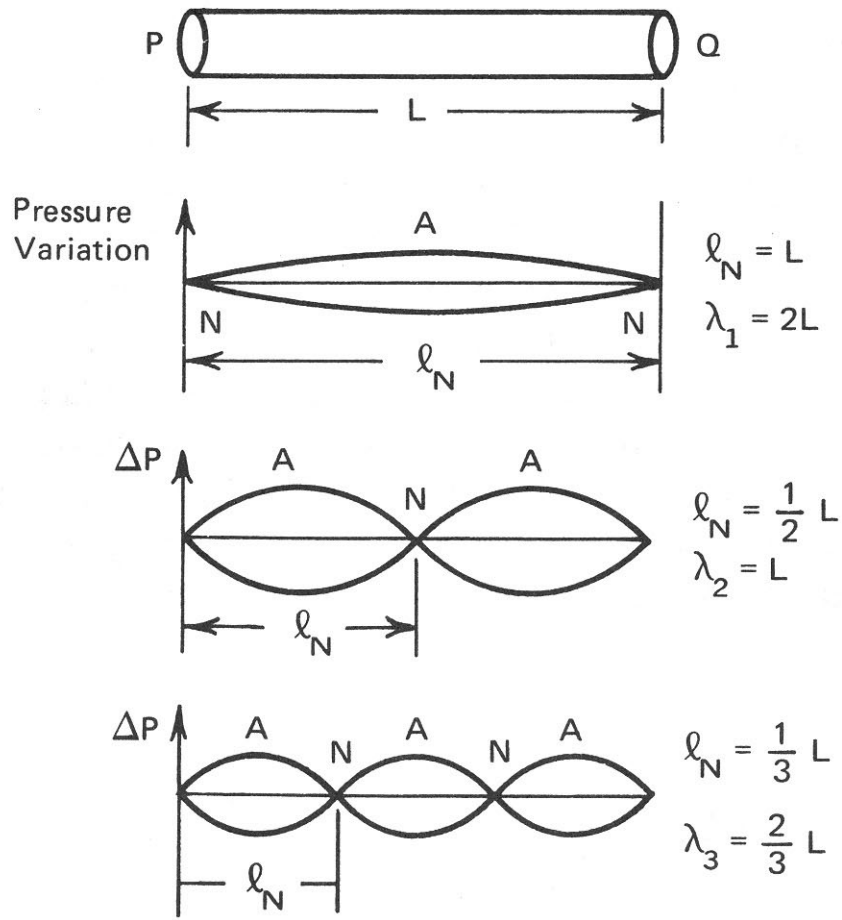

FIGURE 4.17 Standing wave modes (pressure variations) in an idealized cylindrical pipe, open at both ends.

(Roederer, 1994)

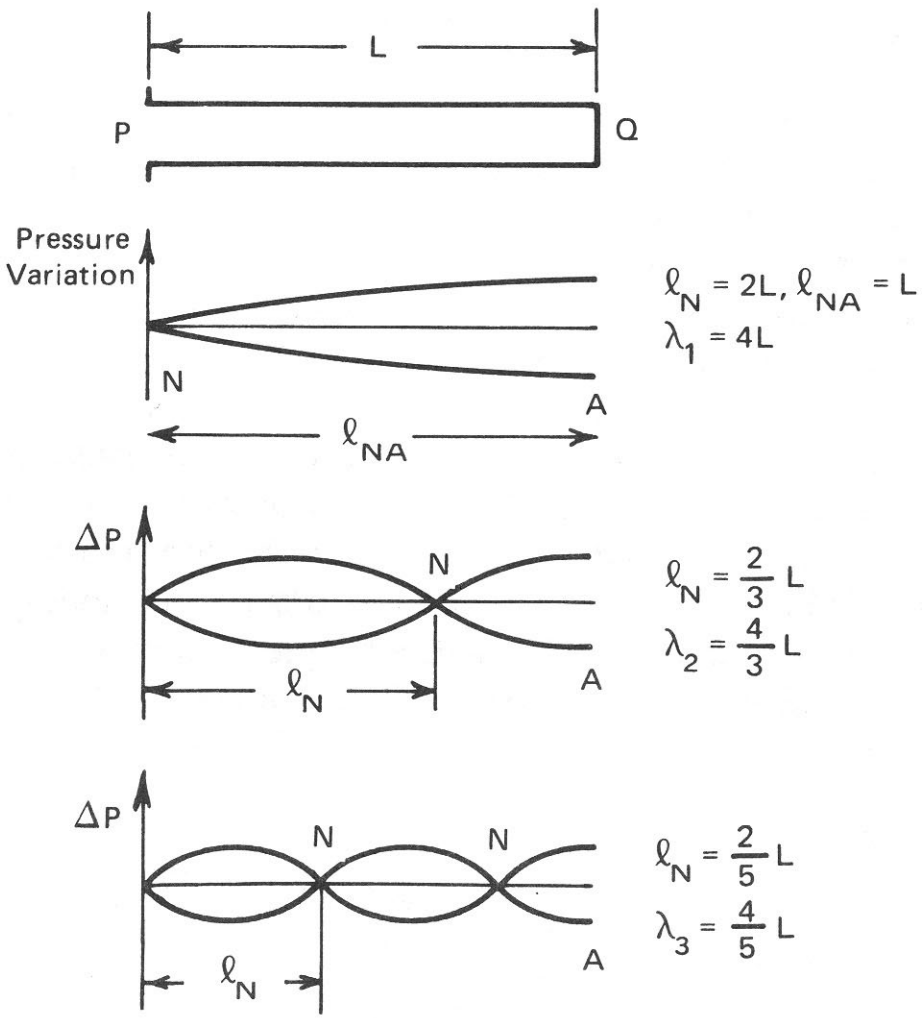

FIGURE 4.19 Standing wave mode in an idealized cylindrical pipe, closed at one end.

(Roederer, 1994)

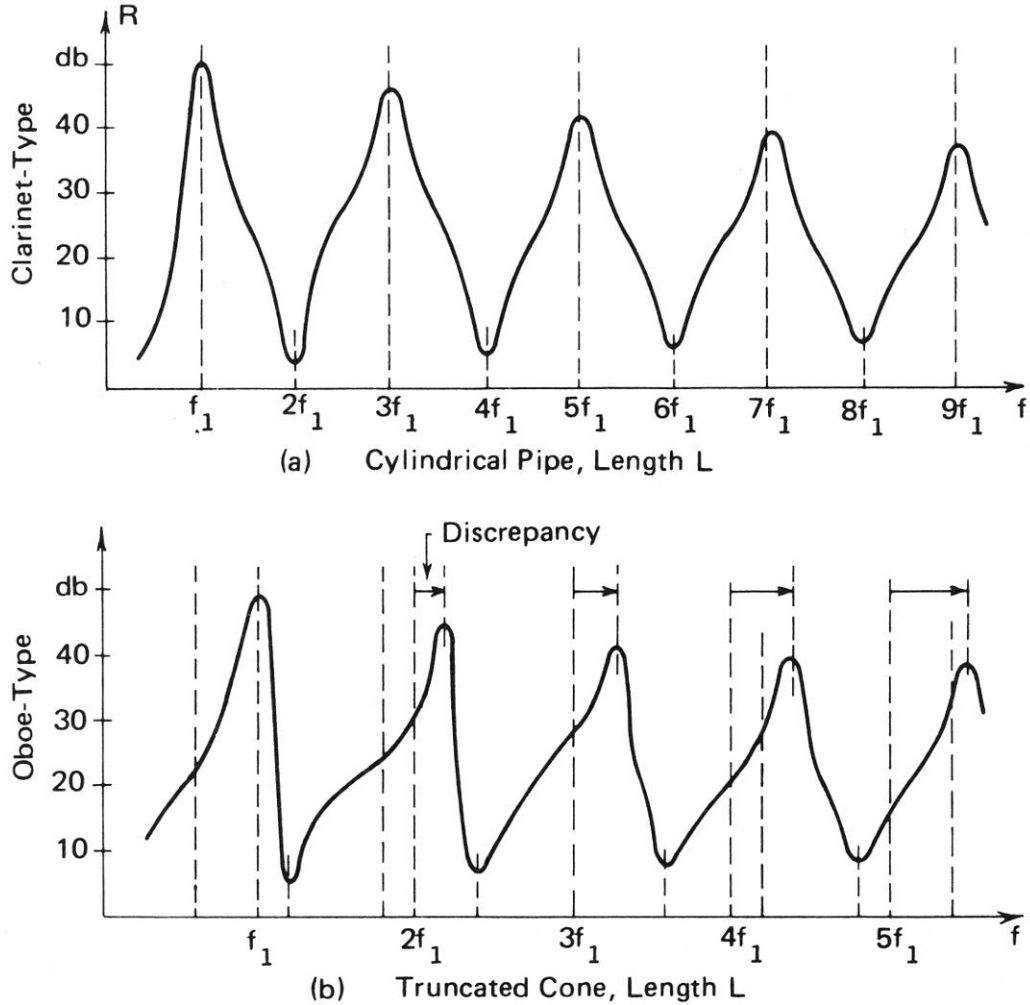

FIGURE 4.24 Typical resonance curves (after Benade, 1971) for clarinet-type (cylindrical) and oboe-type (conical) air columns (without mouthpiece, bell; closed fingerholes).

(Roederer, 1994)

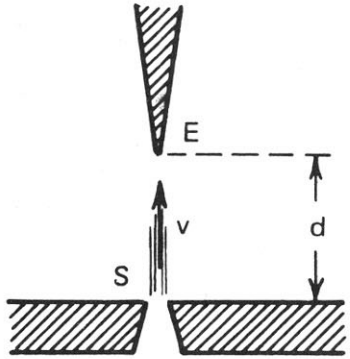

FIGURE 4.22 Generation of an edge tone.

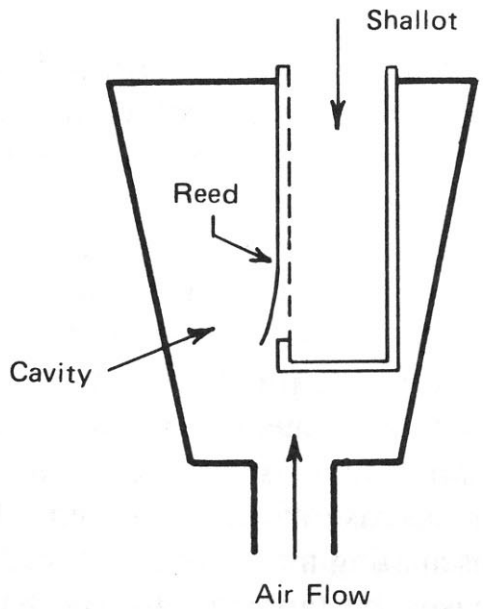

FIGURE 4.23 Reed mechanism for a reed-stop organ pipe.

(Roederer, 1994)

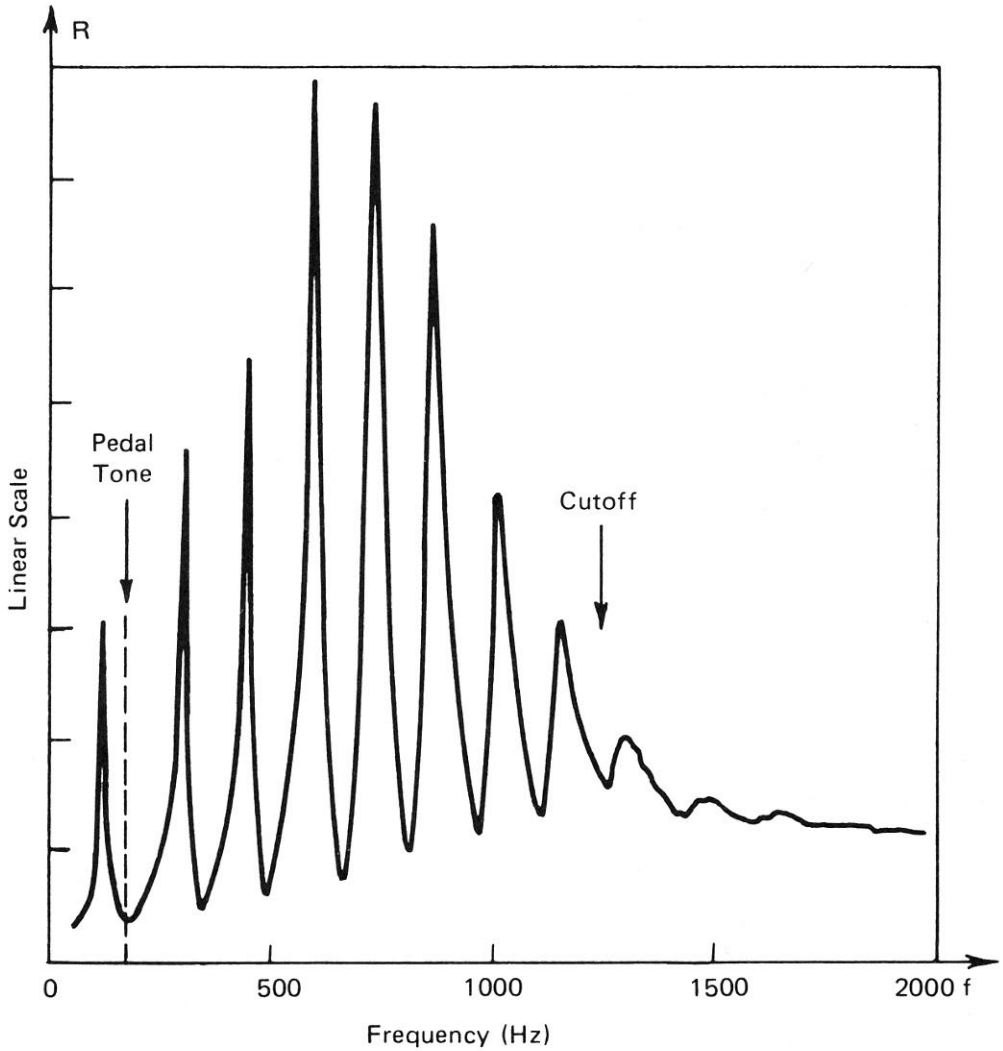

FIGURE 4.25 Resonance curve of a trumpet (Benade, 1971) (given in linear scale).

By permission of Professor A. Benade, Case Western Reserve University, Cleveland, Ohio.

(Roederer, 1994)

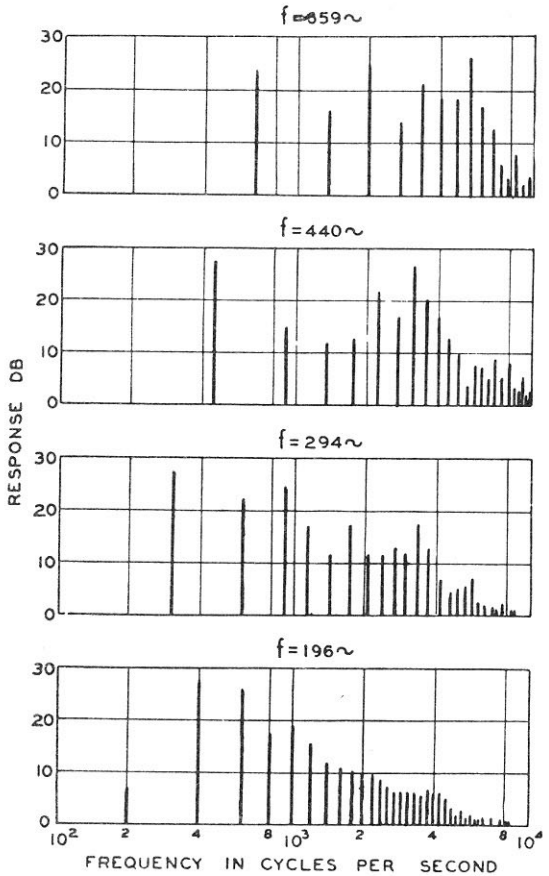

FIG. 6.14. The acoustic spectrums of the four open strings of a violin.

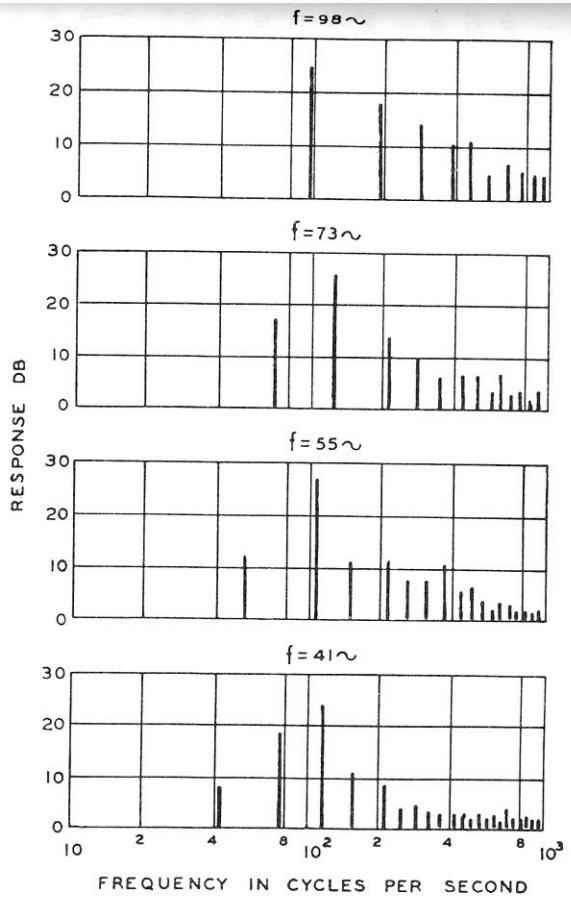

FIG. 6.15. The acoustic spectrums of the four open strings of a double bass.

(Olson, 1967)

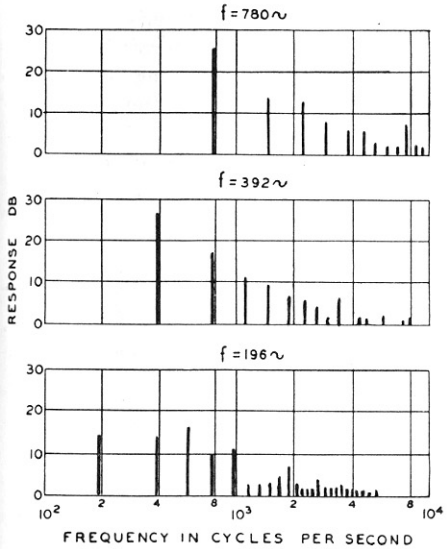

FIG. 6.24. The acoustic spectrums of three tones of an alto saxophone.

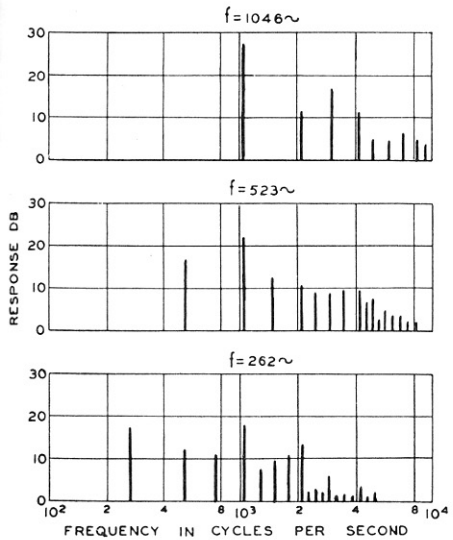

FIG. 6.25. The acoustic spectrums of three tones of an oboe.

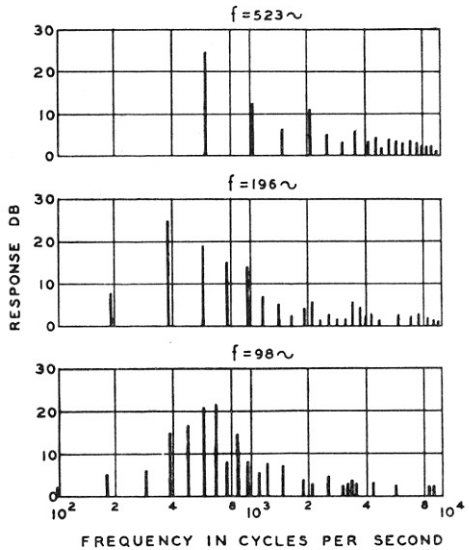

FIG. 6.26. The acoustic spectrums of three tones of a bassoon.

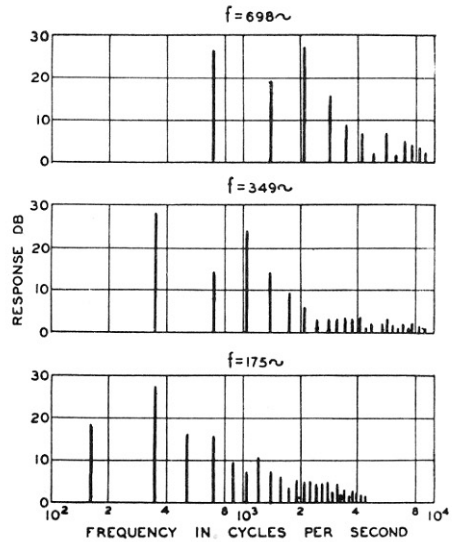

FIG. 6.27. The acoustic spectrums of three tones of a trumpet.

(Olson, 1967)

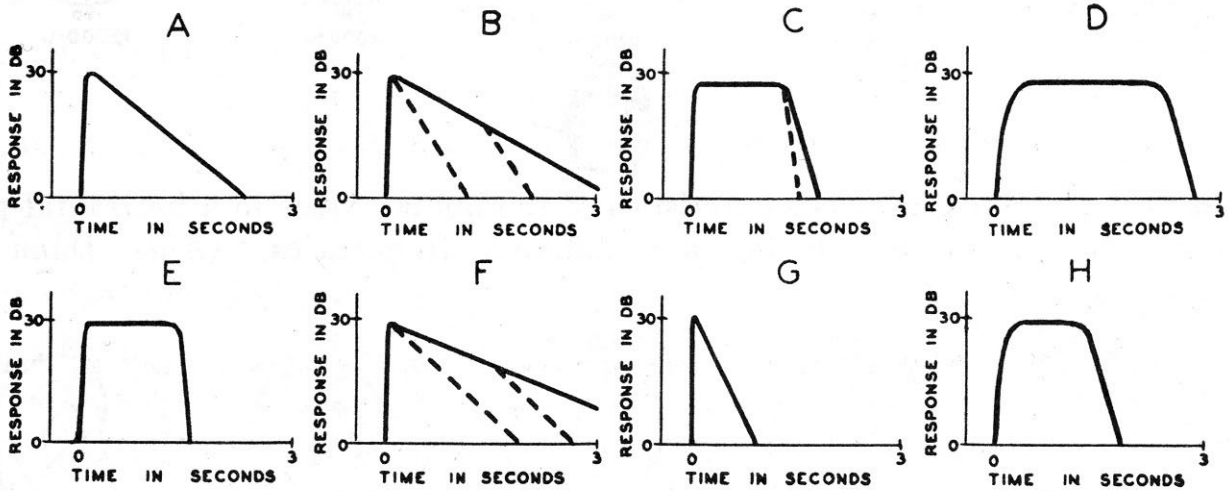

FIG. 6.45. Growth, steady-state, and decay characteristics of various musical instruments. *A*. Plucked-string instruments. *B*. Struck-string instruments. *C*. Bowed-string instruments. *D*. Flue organ pipe. *E*. Air-, mechanical-, and lip-reed instruments. *F*. Percussion instruments of definite pitch. *G*. Drums. *H*. Voice vowel sounds.

(Olson, 1967)

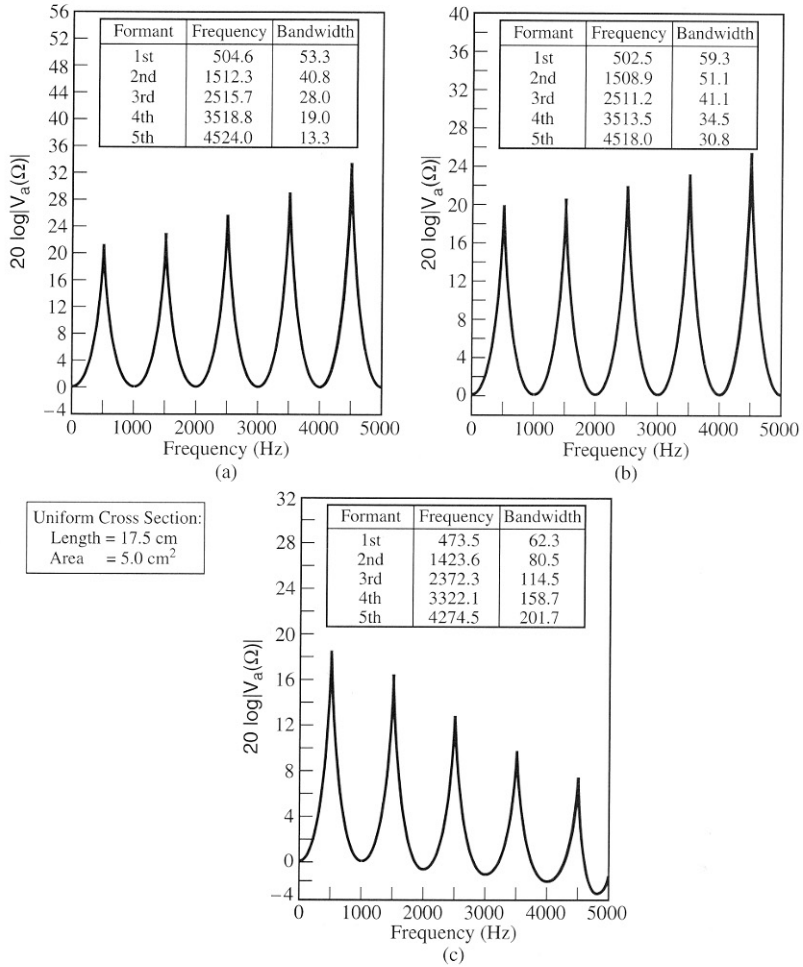

Figure 4.10 Frequency response of uniform tube with (a) vibrating walls with $p(l, 0) = 0$; (b) vibrating walls, and viscous and thermal loss with $p(l, 0) = 0$; (c) vibrating walls, viscous and thermal loss, and radiation loss [26],[28]. 3 dB bandwidths are given.

SOURCE: M.R. Portnoff, *A Quasi-One-Dimensional Digital Simulation for the Time-Varying Vocal Tract* [26]. ©1973, M.R. Portnoff and the Massachusetts Institute of Technology. Used by permission.

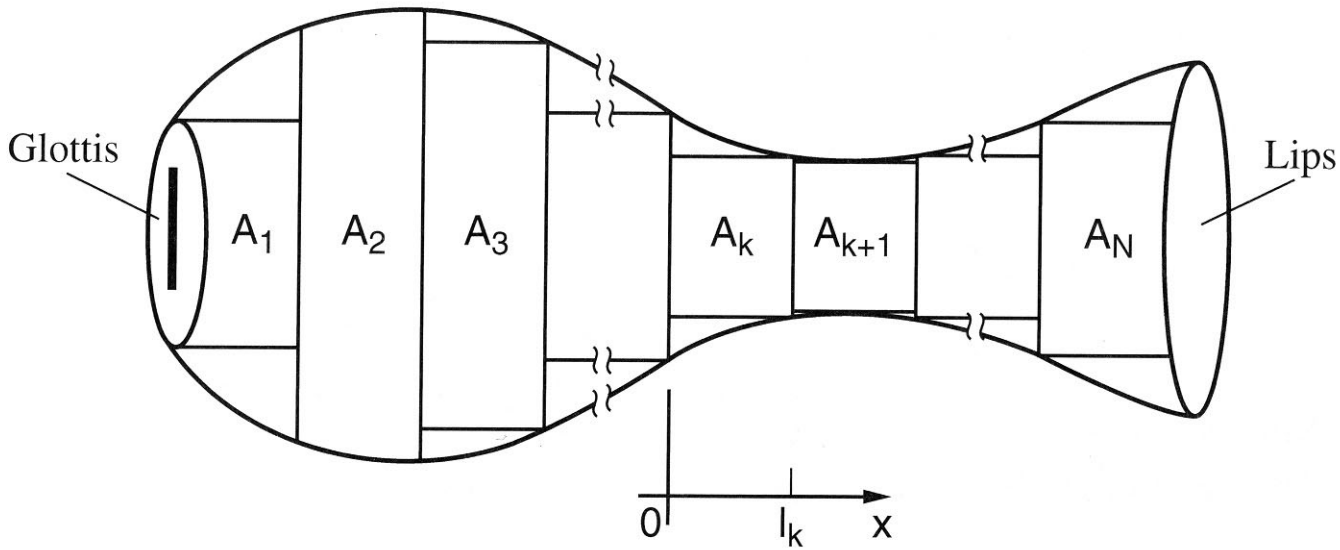

Figure 4.14 Concatenated tube model. The kth tube has cross-sectional area A_k and length l_k.

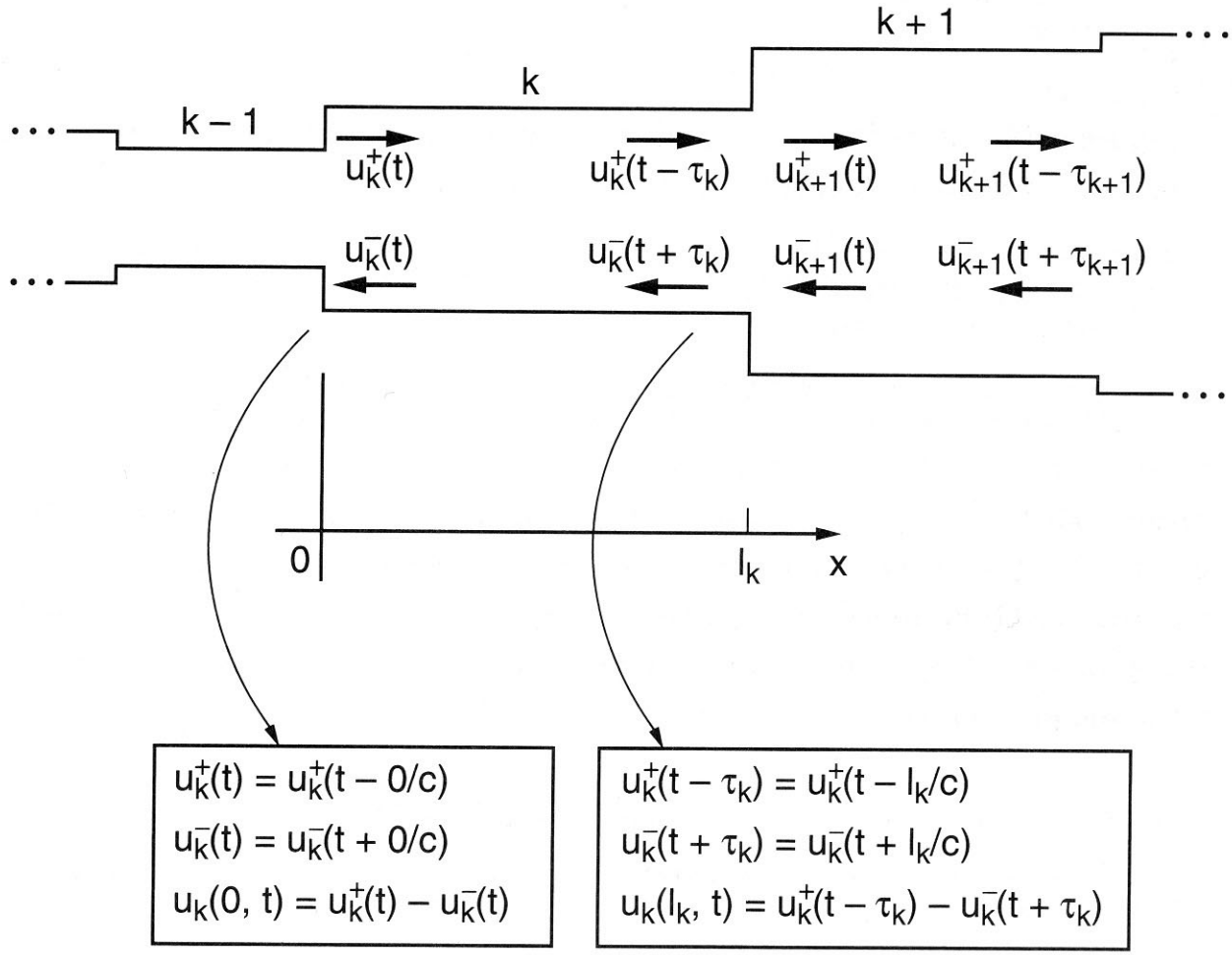

Figure 4.15 Sound waves in the concatenated tube model consist of forward- and backward-going traveling waves that arise from reflection and transmission at a tube junction.

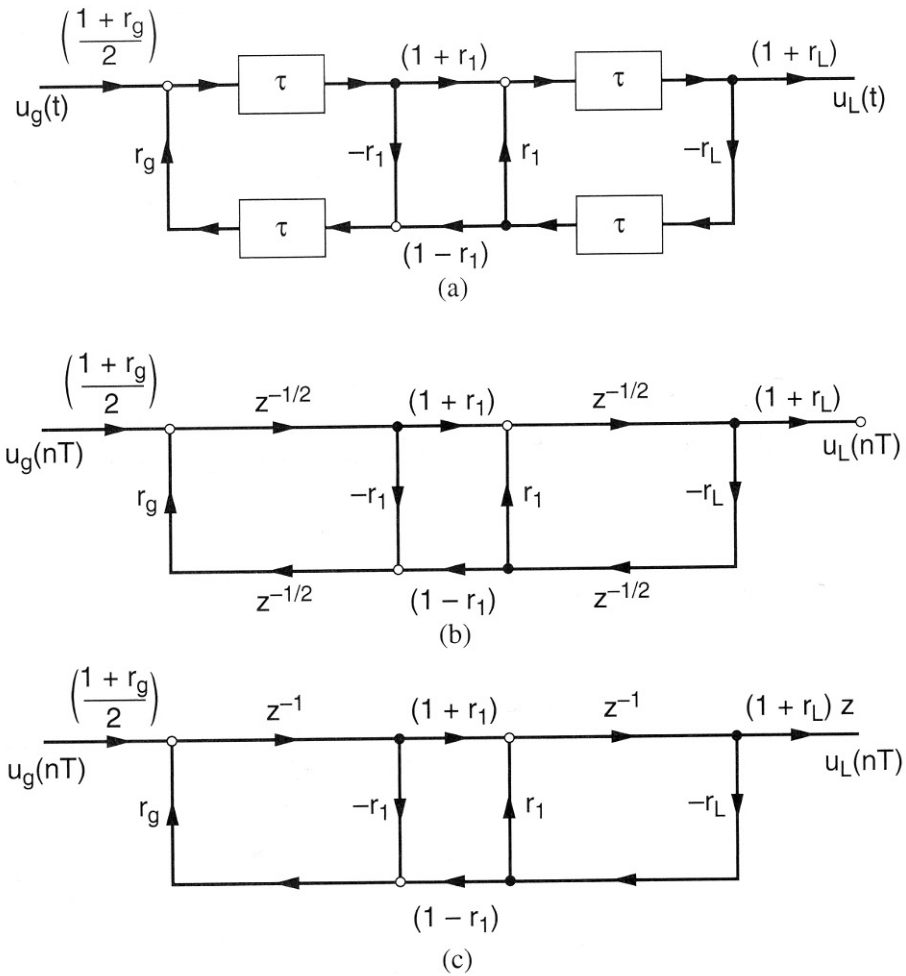

Figure 4.18 Signal flow graph conversion to discrete time: (a) lossless two-tube model; (b) discrete-time version of (a); (c) conversion of (b) with single-sample delays.

SOURCE: L.R. Rabiner and R.W. Schafer, *Digital Processing of Speech Signals* [28]. ©1978, Pearson Education, Inc. Used by permission.

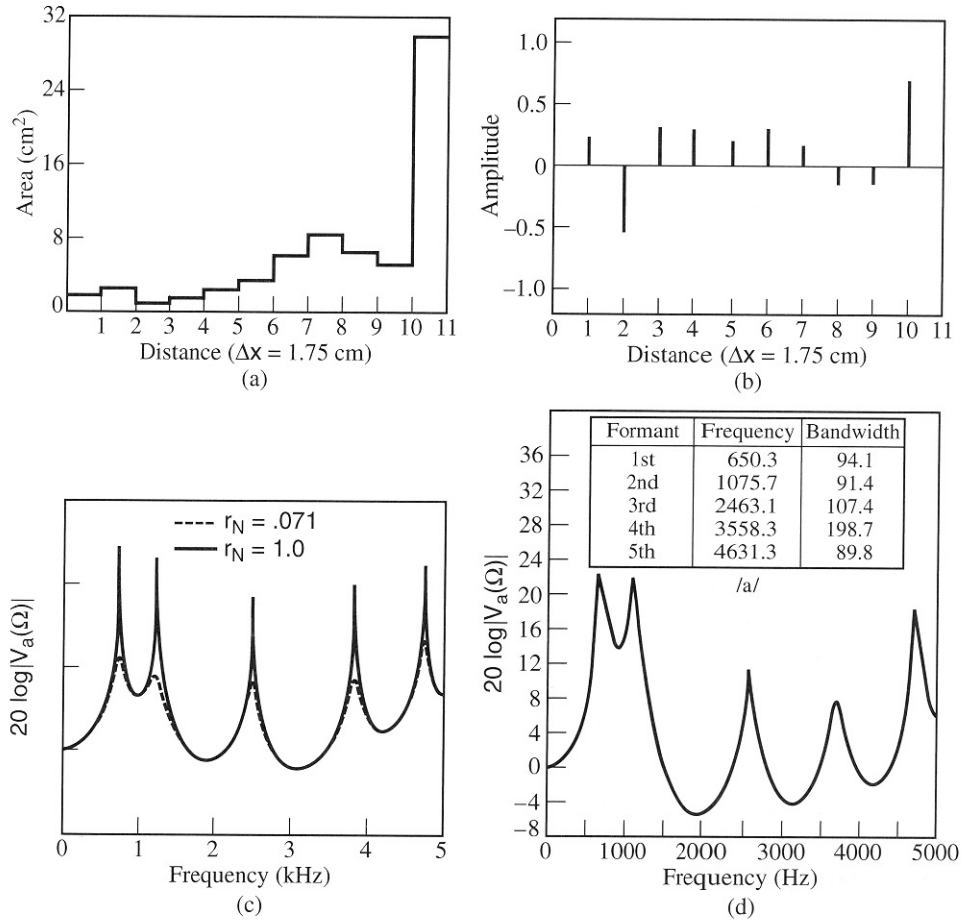

Figure 4.19 Comparison of the concatenated tube approximation with the "exact" solution for area function (estimated by Faut [7]) of the Russian vowel /a/ [26],[28]: (a) cross-section $A(x)$ for a vocal tract model with 10 lossless sections and terminated with a 30 cm^2 section that does not reflect; (b) reflection coefficients r_k for 10 sections; (c) frequency response of the concatenated tube model—the solid curve corresponds to the lossless termination (zero bandwidths) and the dashed curve corresponds to the condition with loss (finite bandwidths); (d) frequency response derived from numerical simulation of Portnoff.

SOURCE: M.R. Portnoff, *A Quasi-One-Dimensional Digital Simulation for the Time-Varying Vocal Tract* [26].

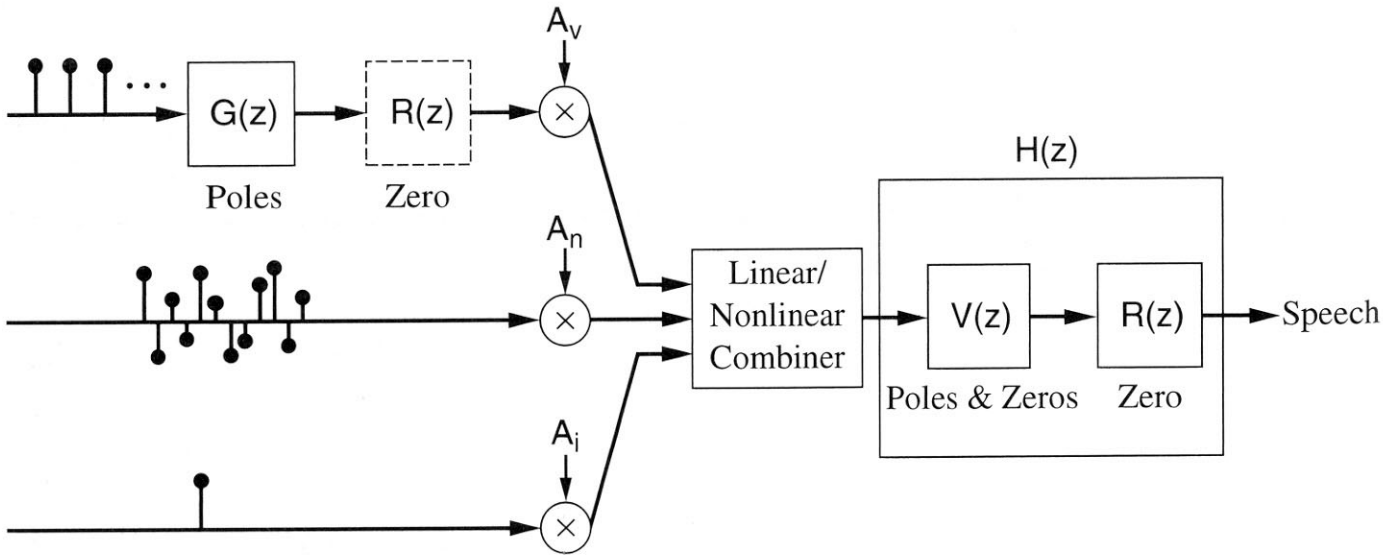

Figure 4.20 Overview of the complete discrete-time speech production model.

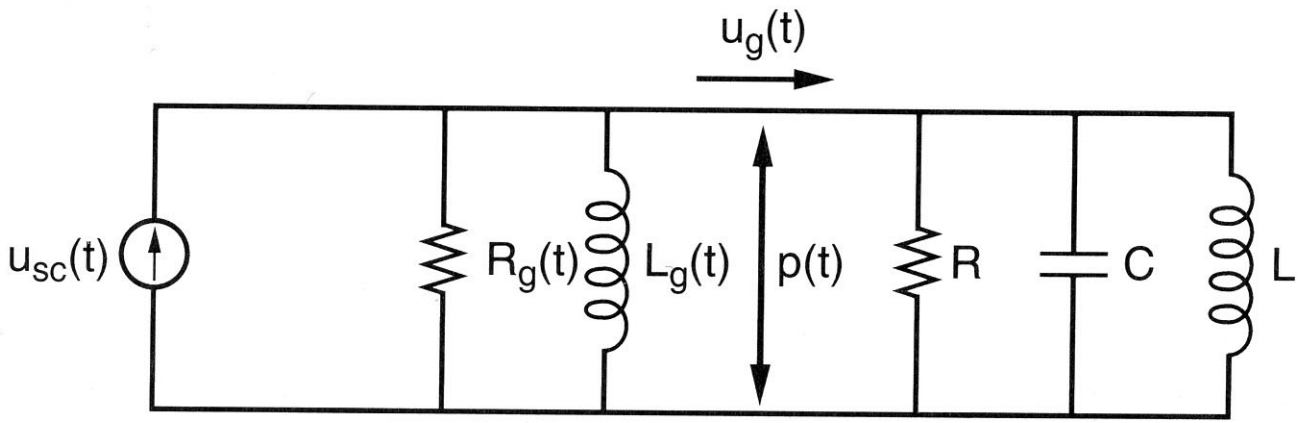

Figure 4.24 Transformed vocal fold/vocal tract first-formant interaction model that is Norton equivalent to circuit of Figure 4.22.

SOURCE: C.R. Jankowski, *Fine Structure Features for Speaker Identification* [10].